Journal of Materials Chemistry A

Accepted Manuscript

ROYAL SOCIETY OF CHEMISTRY

www.rsc.org/materialsA

Journal of
Materials Chemistry A

PAPER

A post-grafting strategy to modify g-C_3N_4 with aromatic heterocycles for enhanced photocatalytic activity

Received 00th January 20xx,
Accepted 00th January 20xx

DOI: 10.1039/x0xx00000x

www.rsc.org/

Jianjian Tian,[a,b] Lingxia Zhang,*[b] Xiangqian Fan,[b] Yajun Zhou,[b] Min Wang,[b] Ruolin Cheng,[b] Mengli Li,[b] Xiaotian Kan,[b] Xixiong Jin,[b] Zhenghao Liu[b,c], Yanfeng Gao,*[a] Jianlin Shi*[b]

A novel and facile post-grafting strategy, instead of conventional copolymerization, via Schiff base chemical reaction between aldehyde and -NH_2 groups has been developed to construct aromatic heterocycle-grafted graphitic carbon nitride (g-C_3N_4) photocatalysts for the first time. The high-resolution N 1s XPS spectrum and the CO_2 TPD analysis confirmed the successful introduction of heterocycles and the reduced structure defects (unreacted -NH_2 groups during the copolymerization formation of g-C_3N_4). The post-grafting of aromatic rings into g-C_3N_4 network did not disrupt the original framework of g-C_3N_4, but effectively expanded its π-delocalized system, enlarged its surface area and promoted the separation and transfer of photo-excited charge carriers. As a result, the obtained copolymer composites exhibit significantly enhanced visible-light photocatalytic activity for H_2 evolution over the pristine g-C_3N_4. This strategy is general and can be used to graft numbers of aromatic rings of different molecular structures onto g-C_3N_4.

1. Introduction

Global energy shortage and environmental pollution stimulates scientists to explore new clean and sustainable energies that may replace fossil fuels. Semiconductor-mediated harvest and conversion of solar energy through water photolysis to produce hydrogen has been considered as a sustainable and prospective solution to alleviate the energy crisis and environmental issues.[1, 2] Various semiconductors or their composite materials have been developed as possible photocatalysts in past decades.[3-5] Recently, graphitic carbon nitride (g-C_3N_4), a metal-free photocatalyst, has attracted intensive interest. In detail, g-C_3N_4 has a bandgap of ca. 2.7 eV and consequently can absorb light up to 450 nm.[6] Its suitable band gap, together with its thermal and chemical stability, is especially suitable for applications in photochemistry and photocatalysis. However, it still suffers from a high recombination probability of photoexcited charge carriers (electron-hole), inefficient utilization of visible-light and thus low photocatalytic conversion efficiency.[7] To overcome this problem and improve its photocatalytic performance, numerous methods have been developed, such as synthesizing mesoporous structures[6, 7] or nanocomposite structures,[10] introducing heteroatoms,[11-14] copolymerization,[15] coupling with dyes[16] or other semiconductors[8] etc.

Among the various strategies, copolymerization with organic monomers or constructing polymer-polymer composites can effectively modify the electronic properties of this π-conjugated polymer.[15] Hao et al[9] adopted a facile one-step thermal condensation to synthesize PAN/g-C_3N_4 composites and effectively improved the interfacial charge transfer. Zhu et al[20] fabricated P3HT-g-C_3N_4 heterojunction by assembling p-type P3HT particles on n-type g-C_3N_4 nanoplates via a ball milling method. The photocatalytic activity was enhanced since the addition of P3HT increased the π-conjugated length of g-C_3N_4 network. Zhang et al[21] incorporated a little amount of pyrimidine rings into the network of g-C_3N_4 to substitute one nitrogen atom with carbon atom in the tri-s-triazine ring. Wang et al[21-24] grafted aromatic motifs into the conjugated g-C_3N_4 networks via one-pot co-condensation of urea (or dicyandiamide) and organic co-monomers (such as 2,4-diaminoquiazoline, 2-aminothiophene-3-carbon-itrile, barbituric acid, diaminomaleonitrile, thiophene etc.). It is conducive to extend the delocalization of π electrons, change the intrinsic semiconductor properties, and consequently, greatly improves the photocatalytic activity of g-C_3N_4. Our group[10, 11]constructed g-C_3N_4-based copolymers via nucleophilic substitution/addition reaction between aromatic bromides and urea or schiff base chemical reaction between aromatic aldehydes and urea, respectively. All the as-synthesized copolymers showed remarkably enhanced and stable visible-light photocatalytic hydrogen evolution performance. However, organic monomers copolymerization with active groups of precursors may form interface defects (e.g. -NH groups) and destroy reactive centers, which cause polymer growth terminated and tri-s-triazine network interrupted at some point. The reduced

[a] School of Materials Science and Engineering, Shanghai University, 99 Shangda Road, Shanghai, 200444, P.R. China
[b] State Key Laboratory of High Performance Ceramics and Superfine Microstructure, Shanghai Institute of Ceramics, Chinese Academy of Sciences, Shanghai, 200050, P.R. China
[c] School of Materials Science and Engineering, Shijiazhuang Tiedao University, 17 Northeast, Second Inner Ring, Shijiazhuang, 050043, P.R. China
E-mail: zhlingxia@mail.sic.ac.cn; yfgao@shu.edu.cn; jlshi@mail.sic.ac.cn; Fax: +86 21-52413122

† Electronic Supplementary Information (ESI) available: scheme of the synthesis of CNTE-x sample, XRD patterns, FT-IR spectra the corresponding band gap of CN, CNTE-x, fresh CNTE-1 and used CNTE-1 samples, O 1S XPS spectra, Zeta potentials and Mott–Schottky plots collected of CN and CNTE-1, The BET surface area ratios and H_2 evolution rate ratios of CNTN-x/CN, XRD patterns, FT-IR spectra, UV-vis absorption spectra, PL spectra, pore size distributions and Hydrogen evolution rates of CN and CN-250. See DOI: 10.1039/x0xx00000x

polymerization degree of g-C_3N_4 shows a decrease the photocatalytic activity.

As is well known that, there are abundant residual amino groups on the g-C_3N_4 frameworks due to the incomplete condensation of the precursors such as urea, cyanamide, or melamine etc.[27] Guo et al[28] found that the photocatalytic activity of g-C_3N_4 for hydrogen evolution decreased with the increase of $–NH_2$ content. These surface exposed terminal $–NH_2$ groups have been regarded as defects, where the charge carriers recombine during the photocatalytic reaction. Lowering the defect content in g-C_3N_4 is therefore conducive to improve its photocatalytic performance. Fortunately, $–NH_2$ groups are very reactive and can participate in many types of reactions. It means that we can diminish this kind of defect to a large extent in g-C_3N_4 based on suitable amino chemical reactions. Wang et al[29] synthesized PNA–g-C_3N_4 through post-treatment via the hydrogen bonding interaction of p-nitrobenzoic acid (PNA) and g-C_3N_4 to improve the photo-degradation property for methyl orange. However, such a weak binding force is unstable and easily broken.

Here in this work, we have successfully developed a series of novel g-C_3N_4-based composite photocatalysts based on the Schiff base interaction of aldehyde groups and surface exposed terminal amino groups in g-C_3N_4 after the thermal polymerization of urea was complete. In this way, π-delocalized system of g-C_3N_4 has been expanded by the grafted aromatic rings through covalent C=N bond. In the mean time, the amount of the residual amino groups has been largely reduced. As expected, compared with the pristine g-C_3N_4, the obtained composites show remarkably enhanced photocatalytic H_2 evolution performance by water-splitting under visible light. According to our knowledge, this is the first report on the covalent post-grafting modification of g-C_3N_4, instead of most reported copolymerization approaches, for improved visible-light photocatalytic hydrogen evolution.

2. Experimental and theoretical methods

2.1 Chemicals and reagents.

Urea (>99%) was purchased from Sinopharm Chemical Reagent Co,.Ltd.; terephthalaldehyde (>98%), 2-naphthaldehyde (>98%), phenanthrene-9-carboxaldehyde (>97%), pyrrole-2-carboxaldehyde (>98%), indole-3-carboxaldehyde (>98%), 2-quinolinecarboxaldehyde ($C_{10}H_7NO$) (>96%) and benzo[b]thiophene-3-carboxaldehyde (C_9H_6OS) (>98%) were purchased from TCI Co., Ltd.; 2,5-thiophenedicarboxaldehyde ($C_6H_4O_2S$) (>99%), triethanolamine (>97%) and chloroplatinic acid hexahydrate (>37.5%, Pt basis) were purchased from Sigma–Aldrich Co., LLC. All chemicals were used as received without further purification.

2.2 Sample preparation.

2.2.1 Preparation of g-C_3N_4. Sample g-C_3N_4 was prepared by thermally decomposing urea at 550 °C in an alumina crucible with a cover for 2 h in static air with a ramp rate of 5 °C min^{-1}. Then, the crucible was cooled to room temperature naturally. The resulting yellow product was collected and ground into fine powder for further use and was denoted as CN.

2.2.2 Post-grafting modification of g-C_3N_4. Various aromatic aldehydes were used to post-modify g-C_3N_4. Taking terephthalaldehyde as an example, in a typical procedure, 1 g of g-C_3N_4 and a certain amount of terephthalaldehyde were mixed thoroughly. Then the mixture was put in an alumina crucible with a cover and heated to 250 °C (the boiling point temperature of aromatic aldehydes) for 5 h at a heating rate of 5 °C min^{-1} in air. The products were denoted as CNTE-x, in which x respects the weight percentage of terephthalaldehyde in the mixture (x% = 0.1, 0.5, 1, 5 and 10%).

2.2.3 Post-heating treatment of g-C_3N_4. As comparison, the obtained g-C_3N_4 (CN) was heated at 250 °C in an alumina crucible with a cover for 5 h in static air with a ramp rate of 5 °C min^{-1}. The resulting product was denoted as CN-250.

2.2.4 Copolymerization modification of g-C_3N_4. For comparison, aromatic ring copolymerized g-C_3N_4 was synthesized according to our earlier report.[21] Typically, 20 g urea and 2 mg terephthalaldehyde were mixed thoroughly and then the mixture was put in an alumina crucible with a cover and heated to 550 °C for 2 h at a heating rate of 5 °C min^{-1}. The resulting product was denoted as CNAL-2.

2.3 Characterization.

Elemental analysis (C, H, N) was performed on a Vario EL microanalyzer. X-ray diffraction (XRD) measurements were conducted on a Rigaku D/Max 2200PC diffractometer (Cu Kα radiation). Fourier transformed infrared (FTIR) spectra were recorded with a Nicolet iS10 FTIR spectrometer. X-ray photoelectron spectroscopy (XPS) measurement was carried out on a Thermo Scientic Escalab 250 spectrometer with Al Kα radiation as the excitation source. Binding energies for the high resolution spectra were calibrated by setting C 1s to 284.6 eV. Transmission electron microscopy (TEM) images and electron energy loss spectroscopy (EELS) results were obtained with a FEI Magellan 400 instrument. The BET surface areas were measured on a Micromeritics Tristar 3000 system. The UV-visible absorption spectra were recorded in the range of 300-800 nm with a UV-3600 PC Shimadzu spectroscope using $BaSO_4$ as a reference. Photoluminescence spectra (PL) of the samples were obtained at room temperature excited by incident light of 380 nm using a fluorescence spectrometer (Shimadzu RF-5301PC). The temperature-programmed desorption of CO_2 (CO_2-TPD) was carried out on a Micromeritics Chemisorb 2750. The zeta potentials of the samples in water were measured using a Zetasizer nano ZS90 analyzer (Malvern Instruments Ltd., UK).

2.4 Electrochemical Analysis.

Electrochemical measurements were conducted on a CHI 760E electrochemical workstation (Chenhua Instruments, Shanghai, China) with a standard three-electrode cell, which employed an FTO electrode deposited with samples as the working electrode, a platinum sheet as the counter electrode and saturated Ag/AgCl as the reference electrode. A 300 W Xe lamp (PLS-SEX300C, Perfectlight Limited, Beijing) with a 420 nm cut-off filter was used as visible light source. The working electrodes were prepared by electrophoretic deposition in an acetone solution (25 mL) containing sample powder (20 mg) and iodine (40 mg). The FTO

glass was kept in the above solution for 5 min with a 10 V bias under potentiostat control. After being calcined for 2 h in an oven at 150 °C, a homogeneous film was obtained. 50 mL of 0.2 M Na_2SO_4 was used as electrolyte solution, which represented the best compromise between activity and stability of the composites.

2.5 Photocatalytic hydrogen evolution test.

The visible light-induced H_2 evolution was carried out in a Pyrex top-irradiation reaction vessel connected to a closed glass gas-circulation system (Lab-Solar-III AG, Perfectlight Limited, Beijing). A 300 W xenon lamp (CEL-HXF300, Ceaulight, Beijing) with a 420 nm cut-off filter was chosen as a visible light source, and the light intensity was 230 mW cm^{-2} (tested by FieldMaxII-TO, Coherent). Photocatalyst (100 mg) was suspended in an aqueous solution (100 mL) containing triethanolamine (10 vol %), and 3 wt% Pt was loaded on the surface of the catalyst by in situ photodeposition using H_2PtCl_6 as the precursor. The reactant solution was evacuated several times to remove air prior to the irradiation experiment. The temperature of the reaction solution was maintained at 10 °C by a flow of cooling water during the photocatalytic reaction. The evolved gases were analyzed by gas chromatography (GC7900, Techcomp) equipped with a thermal conductive detector (TCD) and a 5 Å molecular sieve column, using nitrogen as the carrier gas.

3. Results and discussion

The post-grafting incorporation of aromatic rings into the conjugated system of g-C_3N_4 based on Schiff base reaction of aromatic aldehydes and the terminal –NH_2 groups is depicted in Fig. S1. The g-C_3N_4 sample was synthesized by the thermal polymerization of urea at elevated temperature. Because of the kinetic problems during the thermo-polymerization process of urea, it is difficult to obtain ideally condensed and completely crystallized g-C_3N_4 phase, leaving a number of -NH_2 groups at the edge of s-triazine ring (Fig. S1A). Then aldehyde groups in terephthalaldehyde can be subjected to schiff base reaction with the marginal –NH_2 groups in g-C_3N_4 to form C=N bonds. Consequently, benzene rings can be grafted onto g-C_3N_4 network by dint of this chemical post-grafting method, creating surface/interfacial heterojunctions as well as reducing amino defects. Results of elemental analysis are shown in Table 1, as expected, the molar ratio of C to N gradually increases with more benzene rings being incorporated. For example, the C/N molar ratio increases from 0.692 of the pristine g-C_3N_4 (CN) to 0.717 of CNTE-10, indicating successful grafting of benzene rings into the network of g-C_3N_4.

The X-ray diffraction (XRD) patterns of CN and CNTE-x samples are showed in Fig. S2a. All the samples exhibit two distinct diffraction peaks, which can be ascribed to the typical diffraction peaks of g-C_3N_4, indicating that the molecular framework of g-C_3N_4 has been well retained after the post-grafting modification. The stronger peak at around 27.6° represents the (002) interlayer reflection of the graphitic-like structure with d=0.322 nm.[30] The other small reflection peak at about 12.8° is attributed to the (100) inplane repeated units of tri-s-triazine. Notably, the (002) peak has shifted from 27.68° to 27.58° with the gradual increase of benzene ring content, corresponding to the increase of the interplanar distance from 0.322 nm of CN to 0.323 nm of CNTE-10. This indicates that the post-grafted benzene rings have led to slightly expanded packing of the graphitic-like g-C_3N_4 layers. This increase in the interplanar distance may improve the accessibility of the active sites on g-C_3N_4 layers thus enhance the photocatalytic activity.[21] Additionally, no apparent diffraction peaks of terephthalaldehyde can be observed in all the CNTE-x samples, suggesting no aggregation of terephthalaldehyde in the g-C_3N_4 matrix.

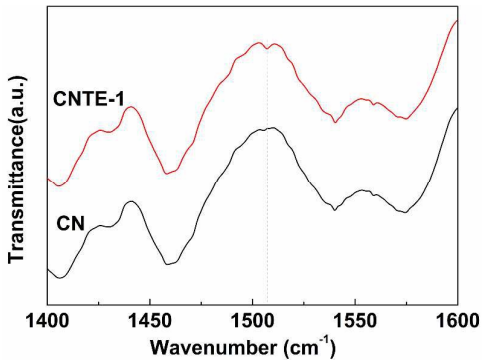

Fig. 1 FT-IR spectra (1400-1600 cm^{-1}) of CN and CNTE-1 samples.

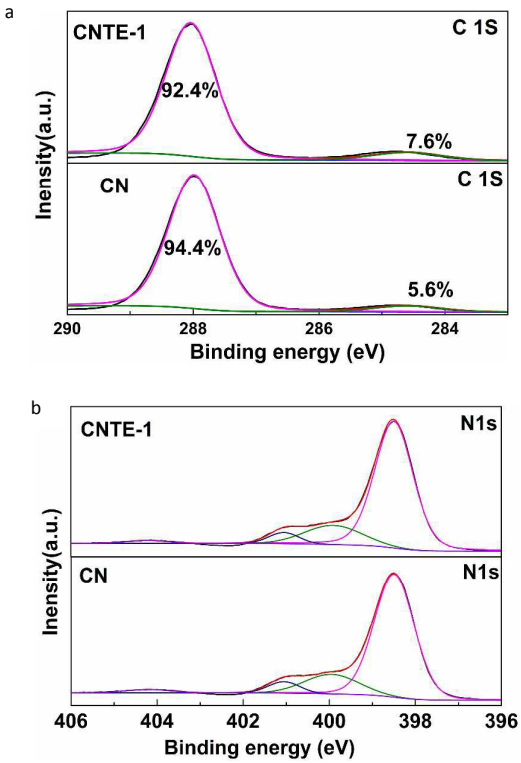

Fig. 2 XPS spectra of CN and CNTE-1, (a) high-resolution C 1s spectra, (b) high-resolution N 1s spectra.

Table 1. Bulk contents of C, N, and H by elemental analysis, textural parameters, and band gap of CN and CNTE-x samples

Sample	C (%)	N (%)	H (%)	C/N atomic ratio	BET (m^2g^{-1})	Pore volume (cm^3g^{-1})	E_g (eV)
CN	35.08	59.16	1.73	0.692	65.20	0.50	2.65
CNTE-0.1	35.27	59.29	1.83	0.694	66.10	0.52	2.64
CNTE-0.5	35.45	59.03	1.77	0.701	83.66	0.61	2.64
CNTE-1	35.80	59.26	1.71	0.705	120.31	0.88	2.62
CNTE-5	35.53	58.39	1.63	0.710	100.28	0.81	2.62
CNTE-10	35.78	58.20	1.63	0.717	98.05	0.81	2.60

Fig. S2b shows the FT-IR spectra of CN and CNTE-x samples. All of the samples exhibit several typical absorption bands revealing the characteristic structure of g-C_3N_4. The intense peak at ca. 810 cm^{-1} is assigned to the out-of-plane deformation vibration modes of s-triazine ring. The multiple bands between 1200-1600 cm^{-1} correspond to the stretching modes of aromatic C-N heterocycle.[12]The broad peaks at around 3100-3400 cm^{-1} are assigned to stretching vibration modes of the -NH group and –OH group of the adsorbed H_2O from air, which become weaker after post-grafting modification, indicating the decreased content of surface amino groups in CNTE-x. Close inspection of the FT-IR spectra reveals noticeable difference between CN and CNTE-1 (Fig. 1). CNTE-1 exhibits a weak IR band located at 1506 cm^{-1}, which is attributed to aromatic C=C bond,[26] further confirming that the aromatic rings have been successfully grafted onto the g-C_3N_4 networks.

In order to further check the chemical nature of the obtained CN and CNTE-1 samples, X-ray photoelectron spectroscopy (XPS) was carried out and the corresponding spectra are shown in Fig. 2. The high-resolution C 1s signals (Fig. 2a) of the two samples can be deconvoluted into two peaks centred at 284.6 and 288.0 eV, which are identified as the aromatic carbon atoms and the sp^2 hybridized carbon in the s-triazine ring, respectively.[13, 14] It is worth noting that the peak at 284.6 eV (i.e. the aromatic carbon atoms, 7.6%) of sample CNTE-1 is much stronger than that of CN (5.6%), suggesting again aromatic rings have been introduced into the g-C_3N_4 matrix. As shown in Fig. 2b, the high-resolution N 1s spectra shows four peaks centred at about 398.5, 399.9, 401.0 and 404.2 eV, respectively. The main signal shows the occurrence of the sp^2-hybridized nitrogen in s-triazine rings (C-N=C, 398.5 eV, N_{2C}) and tertiary nitrogen groups (N-$(C)_3$, 399.9 eV, N_{3C}). Both of them, together with the aforementioned sp^2 hybridized carbon (288.0 eV) constitute the s-heptazine heterocyclic ring units as elementary building blocks of the CN polymers.[34] Another weak peak at 401.0 eV indicates the defective amino groups (C-N-H, N_{1C}), originating from the incomplete condensation of heptazine substructures. In addition, the very weak peak at 404.2 eV is attributed to the charging effect or positive charge localization in the heterocycles. After further analysis of the obtained data, the peak-area ratio of N_{2c} to N_{1c} increases from 14.5 in CN to 15.8 in CNTE-1, suggesting the loss of the amino groups after post-modification. This verifies the supposed reaction mechanism that N_{1c} is most likely to turn to N_{2c} via Schiff base reaction between $–NH_2$ and –CHO groups, as depicted in Fig. S1. Fig. S3 shows the binding energies of O 1s peaks. As expected, there is no C=O signal of the aldehyde groups. The two bands located at 532.1 and 533.4 eV both for CN and CNTE-1 samples, can be ascribed to the adsorbed oxygen species (water[35] and oxygen[33]). These findings are in good consistence with the elemental analysis, XRD and FT-IR results.

Due to the incomplete condensation of urea, there are high amounts of residual $–NH_2$ groups in the polymeric networks of g-C_3N_4, which generally become the recombination sites of photo-generated charge carriers in photocatalytic reactions. These $–NH_2$ groups can also act as Lewis basic sites and adsorb slightly acidic CO_2 molecules.[36] The CO_2 temperature programmed desorption (TPD) measurement was conducted on CN and CNTE-1. As shown in Fig. 3, CN sample shows a larger peak area of CO_2 desorption than CNTE-1, suggesting a decreased content of surface $–NH_2$ groups on CNTE-1 in comparison with CN. We further tested zeta potentials of CN and CNTE-1 samples dispersed in water. Because of the free lone pair electrons on nitrogen atoms, $-NH_2$ groups can act as proton acceptors and acquire positive surface charges.[37] It can be seen from Fig. S4, the zeta potential of CNTE-1 (-41.1 mV) is more negative than that of CN (-22.2 mV). This further proves the significantly decreased content of terminal $–NH_2$ groups after post-grafting aromatic rings. The analyses above support the reaction mechanism depicted in Fig. S1. It can be concluded that the aromatic rings have been successfully grafted onto the molecular structure of g-C_3N_4 by chemical modification.

The morphology of CN, CNTE-1, and CNTE-10 samples were investigated by TEM. As shown in Fig. 4, all samples exhibit typical layered structure. Whereas, after the incorporation of aromatic rings, a curved/distorted structure dominates. The EELS spectra of these samples were collected at the layer edges, where amino groups were located, and the results are summarized in Fig. 4d. Not surprisingly, the C/N atomic ratio increases with the increased incorporation of benzene rings, further indicating the aromatic rings have been hung to the position of surface amino groups. Table 1 show that the specific surface area and pore volume increases firstly and then decreases with the increased amount of grafted aromatics rings. The CNTE-1 sample shows a maximum specific surface area (120.31 $m^2 g^{-1}$), which is remarkably higher than that of CN (65.20 $m^2 g^{-1}$). The increased BET surface area might be attributed to the exfoliation and tailoring of the bulk layered structure of g-C_3N_4 during the post-treatment process. However, grafting excessive aromatic rings may lead to over-distortion or curvature of g-C_3N_4 layers, which decreases the specific surface area.

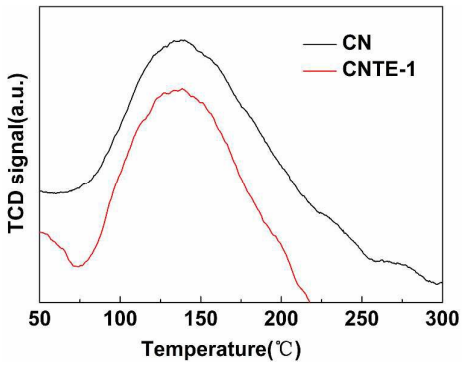

Fig. 3 CO_2 TPD profiles of CN and CNTE-1.

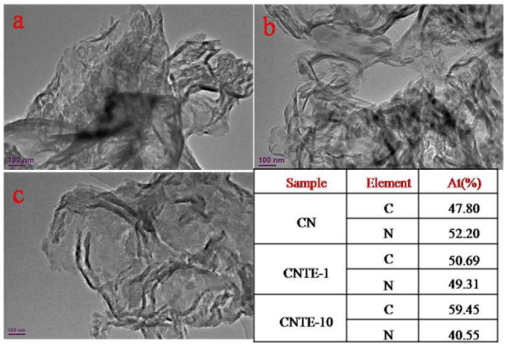

Sample	Element	At(%)
CN	C	47.80
	N	52.20
CNTE-1	C	50.69
	N	49.31
CNTE-10	C	59.45
	N	40.55

Fig.4 Typical TEM images of (a) CN, (b) CNTE-1, and (c) CNTE-10. The table at bottom right summarizes the EELS elemental analysis results conducted at the edge of the lamellas of these samples.

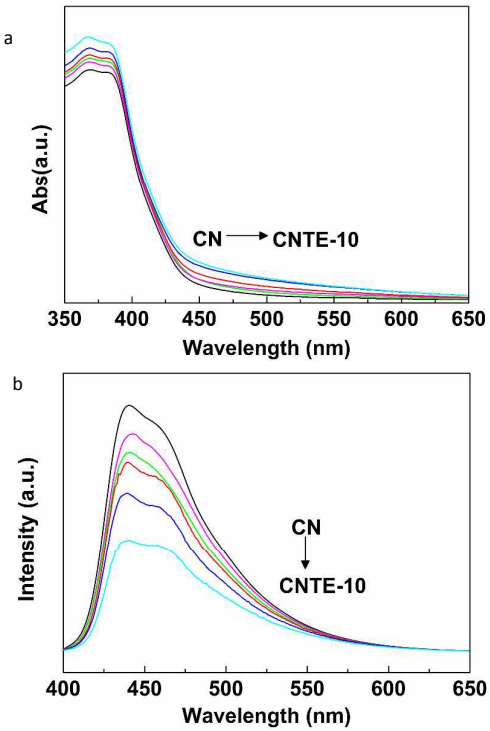

Fig. 5 (a) UV-vis absorption spectra and (b) PL spectra (excitation wavelength: 380nm) of all the samples.

The optical absorptions of CN and CNTE-x composites with different amounts of aromatic rings grafted were characterized using UV-vis absorption spectra. It can be seen from Fig. 5a that, compared with CN, the incorporation of aromatic rings can effectively improve the light absorption in both UV and visible region. Moreover, CNTE-x sample with increased amounts of aromatic rings displays intensified and red-shifted light absorption. This result may be attributed to the following two aspects. One is the extended electron delocalization in the 2D networks of g-C_3N_4 because of the incorporation of aromatic rings[38] and the other is the activation of n to π* electron transition because of the distortion of the co-polymeric units in g-C_3N_4 networks.[39] The band gap of the obtained samples has been estimated by a classical Tauc approach (Fig. S5) and shown in Table 1. E_g value decreases from 2.65 eV of CN to 2.60 eV of CNTE-10, implying that the electronic structure of g-C_3N_4 has been remarkably modified by the grafting of aromatic rings. And at the same time, the visible light harvesting of the photocatalyst has also been enhanced.

Photoluminescence spectra (PL) were performed to determine the separation/recombination of photogenerated charge carriers.[40] In Fig. 5b, the CNTE-x samples have similar PL spectra to CN, but the PL emission intensity of the CNTE-x samples gradually decreases as the amount of grafted aromatic rings increases. Because grafting aromatics into carbon nitride networks can extend conjugated π-electron system and make the carbon nitride layer more curved/distorted. The distortion of CNTE-x layers increases the intramolecular collision frequency, resulting in the rapid loss of exiton energy and the aggravation of PL quenching.[26,38] This indicates that the grafting of aromatic rings has effectively improved the separation of photogenerated charge carriers in the modified g-C_3N_4 photocatalysts under visible-light illumination.[40]

Based on the above discussion, it is safe to conclude that the grafted aromatics onto the g-C_3N_4 framework has brought following benefits for photocatalysis: (1) enlarged specific surface area, which exposes more catalytic active sites; (2) red-shift of absorption edge, which improves the visible light utilization; (3) a lower density of amino defects, which decreases the recombination possibility of charge carriers in photocatalysis reactions. The photocatalytic hydrogen evolution rates of all the samples are presented in Fig. 6a. Significantly enhanced hydrogen evolution rate can be found on all of the CNTE-x samples, especially for CNTE-1, which has the highest photocatalytic performance with a H_2 evolution rate of 92.4 μmol h^{-1}, above 4.1 times that of CN (22.2 μmol h^{-1}) among the samples prepared. When the dosage of terephthalaldehyde is higher than 1 wt%, the photocatalytic H_2 evolution will decrease with the further increased addition of terephthalaldehyde. This can be ascribed to the over-aggravated distortion of g-C_3N_4 layers with more aromatics grafted, resulting in decreased surface area, easier dissipation of photo-generated charge carriers into vibrational or thermal energy, and thus gradually decreased photocatalytic activity. In short, a proper amount of aromatic rings is important to optimize the photocatalytic activity of CNTE-x photocatalysts. Fig. S6 shows that the ratio of BET surface area and the ratio of H_2 evolution rate of CNTE-x/CN evolve in a similar way, indicating that large surface area would benefit the enhancement of photocatalytic performance. However, the H_2 evolution rate normalized to the BET surface area

(H_2 evolution rate ratio/surface area ratio) of CNTE-x (especially CNTE-1) is considerably higher than 1 of CN, suggesting that the surface area can hardly play a decisive role in this photocatalytic system and the other factors also contribute much to the enhanced photocatalytic activity.[25,39] It is well known that the photo-reduction ability of the semiconductor is determined by the potential of its conduction band (LUMO).[42] Based on the Mott-Schottky plots (Fig. S7), the LUMOs of CN and CNTE-1 are estimated to be -1.02 eV and -1.15 eV, respectively. The higher LUMO of CNTE-1 implies the stronger reduction ability of its photo-induced electrons than those in CN. The stability of CNTE-1 has been also demonstrated by repeating the photocatalytic experiments under the same condition for four cycles (16 h) (Fig. 6b). Clearly, there is no significant decrease in the H_2 evolution rate after four consecutive cycles. Furthermore, after photocatalytic reactions, the used CNTE-1 sample was collected by centrifugation. Fig. S8 compares the XRD patterns and FT-IR spectra of CNTE-1 sample before (fresh CNTE-1) and after (used CNTE-1) the photocatalytic reaction. It can be found that, there are no noticeable alternations in the crystal and chemical structure, suggesting the excellent reusability and stability of this photocatalyst.[23]

To further explore how the grafting of aromatic rings promotes the photocatalytic performance of g-C_3N_4, several other analyses were performed to characterize the post-heating treatment sample CN-250. As indicated by XRD, FT-IR, UV-vis absorption, PL spectra and N_2 adsorption-desorption (Fig. S9a-e), the crystal structure, morphology, optical absorption/luminescence properties, the surface areas and pore structures have not changed much after post-heat treatment. For comparison, the photocatalytic H_2 evolution on CN-250 was also examined. Only a very slight improvement in photocatalytic activity was obtained, which is far less significant than that enhanced by the post-grafting of aromatic rings (Fig. S9f). This provides powerful evidences that the remarkably enhanced photocatalytic performance of CNTE-x samples has nothing to do with the post-heating treatment.

The electrochemical impedance spectra (EIS) were recorded to investigate the electrochemical properties of the samples. In general, the radius of the arc reflects the reaction rate on the surface of the electrode. As shown in Fig. 7a, the arc radius of the samples follows the order CN < CNAL-2 < CNTE-1, suggesting that post-grafting modification of g-C_3N_4 can more efficiently promote the separation and transfer of photogenerated charge carriers at the material surface/interface than copolymerization.[43] Both for post-grafting and copolymerization modified g-C_3N_4, surface/interfacial heterojunctions can be created, so the spatial separation of photogenerated charge carriers can be improved. However, during the copolymerization formation of g-C_3N_4, there are more defects derived from incomplete heptazine coupling, which act to increase the charge carrier recombination rate and thus hinder the efficient utilization of charge carriers. In comparison, post-grafting modification of g-C_3N_4 dissipates terminal –NH_2 defects without deceasing its crystallinity, meanwhile, introduces electron acceptors to enhance charge transfer transition[25] and consequently improves the separation/transfer and surface reactivity of charge carriers. Furthermore, the considerably enhanced photocurrent generated (Fig. 7b) on CNTE-1 also indicates the substantially accelerated charge separation and transfer, well in line with the above results.

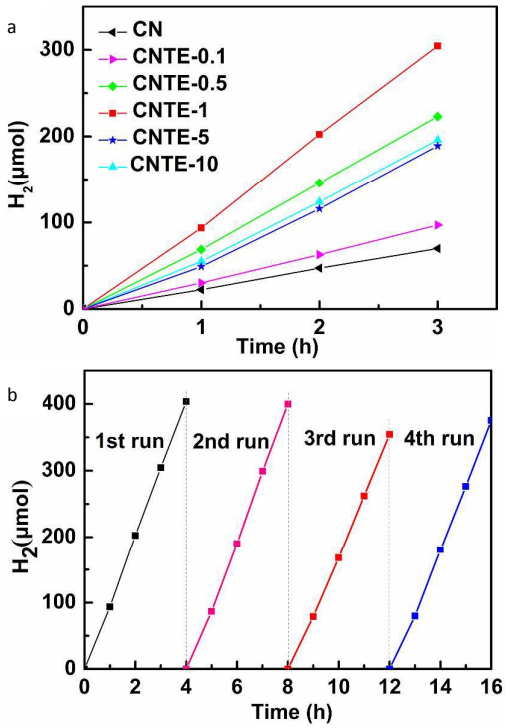

Fig. 6 (a) Hydrogen evolution rates on CN and CNTE-x, (b) Cycling stability test of CNTE-1.

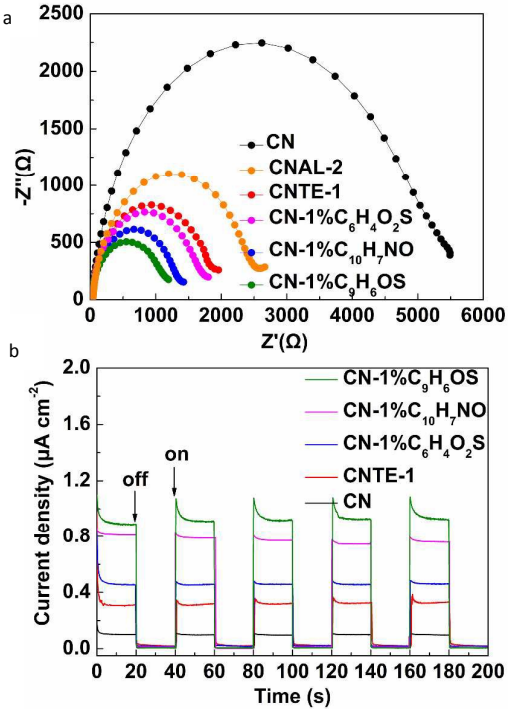

Fig. 7 (a) EIS Nyquist plots in dark and (b) Transient photocurrents under cycling illuminations of CN and CN post-grafted with different aromatic rings (dosage: 1wt% in 1 g g-C_3N_4).

To confirm that the hydrogen evolution reaction is indeed driven by light absorption on the catalyst, wavelength dependence of the photocatalytic H_2 evolution on CNTE-1 was examined using different wavelength optical filters, and its wavelength-dependent apparent quantum yield (AQY) is shown in Fig. 8, which is well coincident with its optical absorption spectrum, suggesting that it is the harvested visible photons that dominate the driving energy force of the photocatalytic reaction.[44]

To illustrate the general feasibility of this post-grafting strategy based on Schiff base chemistry, a series of other aromatic molecules with active aldehyde groups (e.g. 2,5-thiophenedicarboxaldehyde ($C_6H_4O_2S$), 2-quinolinecarboxaldehyde, ($C_{10}H_7NO$) and benzo[b]thiophene-3-carboxaldehyde (C_9H_6OS) etc.), instead of terephthalaldehyde, were chosen as precursors to post-graft other kinds of aromatic rings onto g-C_3N_4 at their individual boiling points. As shown in Fig. 9, all the carbon nitride copolymers incorporated with these aromatic rings show enhanced hydrogen evolution activity. Moreover, the considerably decreased arc radius of Nyquist plots and the enhanced photocurrent of these carbon nitride copolymers，implies their improved electronic conductivity, and the promoited separation and transfer of the charge carriers between them. The photocatalytic activities of these modified carbon nitride polymers are mainly determined by the monocoque of aromatic molecules as well as their optimized dosages.

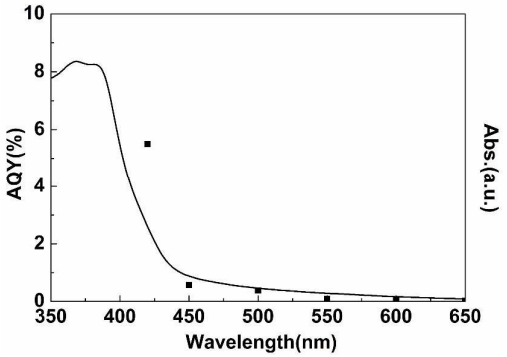

Fig. 8 Wavelength-dependent apparent quantum yield (AQY) on CNTE-1.

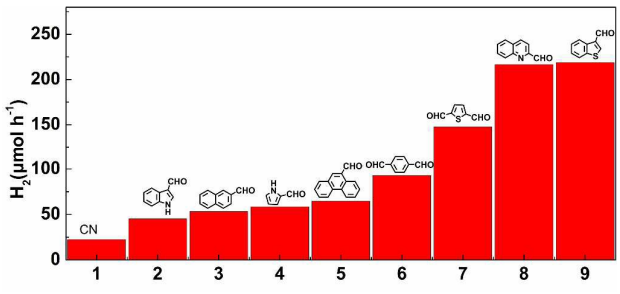

Fig. 9 Hydrogen evolution rates on CN and CN post-grafted with different aromatic rings.

4. Conclusions

A novel post-grafting strategy, rather than copolymerization, based on Schiff base chemistry has been developed to fabricate novel aromatics-grafted carbon nitrides. The introduction of aromatics enables to modifiy the intrinsic electronic properties, enhance the visible light response of g-C_3N_4, and meanwhile, reduce amino defects on its surface, which finally promote the separation and transfer of photogenerated charge carriers and the photocatalytic activity enhancement. Hence the as-obtained copolymers show substantially enhanced photocatalytic hydrogen evolution performance compared with that of the pristine g-C_3N_4. Through this facile strategy, large numbers of aromatics can be grafted onto g-C_3N_4 networks. We anticipate that this post-modification strategy will provide novel routes to construct efficient carbon-nitride-based copolymer photocatalysts with reduced structure defects and enhanced photocatalytic activities.

Acknowledgements

This work was financially supported by the National Key Basic Research Program of China (2013CB933200), National 863 plans projects (2012AA062703), Youth Innovation Promotion Association CAS (2012200), Jiangsu National Synergetic Innovation Center for Advanced Materials (SICAM).

Notes and references

1 G. Zhang, Z.-A. Lan, L. Lin, S. Lin and X. Wang, *Chem. Sci.*, 2016, **7**, 3062.
2 F. Bonaccorso, L. Colombo, G. Yu, M. Stoller, V. Tozzini, A. C. Ferrari, R. S. Ruoff and V. Pellegrini, *Science*, 2015, **347**, 1246501
3 A. Midya, A. Ghorai, S. Mukherjee, R. Maiti and S. K. Ray, *J. Mater. Chem. A*, 2016, **4**, 4534.
4 S. Ghosh, N. A. Kouamé, L. Ramos, S. Remita, A. Dazzi, A. Deniset-Besseau, P. Beaunier, F. Goubard, P.-H. Aubert and H. Remita, *Nat. Mater.*, 2015, **14**, 505.
5 Y. Sang, Z. Zhao, M. Zhao, P. Hao, Y. Leng and H. Liu, *Adv. Mater.*, 2015, **27**, 363.
6 X. Wang, K. Maeda, A. Thomas, K. Takanabe, G. Xin, J. M. Carlsson, K. Domen and M. Antoniett, *Nat. Mater.*, 2008, **8**, 76.
7 J. Fang, H. Fan, Z. Zhu, L. B. Kong and L. Ma, *J. Catal.*, 2016, **339**, 93.
8 X. Bai, L. Wang, R. Zong and Y. Zhu, *J. Phys. Chem. C*, 2013, **117**, 9952.
9 J. Xu, Y. Wang and Y. Zhu, *Langmuir*, 2013, **29**, 10566.
10 H. Wang, Y. Su, H. Zhao, H. Yu, S. Chen, Y. Zhang and X. Quan, *Environ. Sci. Technol.*, 2014, **48**, 11984.
11 T. Y. Ma, J. Ran, S. Dai, M. Jaroniec and S. Z. Qiao, *Angew. Chem., Int. Ed.*, 2015, **54**, 4646.
12 J. Chen, Z. Hong, Y. Chen, B. Lin and B. Gao, *Mater. Lett.*, 2015, **145**, 129.
13 T. Xiong, W. Cen, Y. Zhang and F. Dong, *ACS Catal.*, 2016, **6**, 2462.
14 F. Dong, Z. Zhao, Y. Sun, Y. Zhang, S. Yan and Z. Wu, *Environ. Sci. Technol.*, 2015, **49**, 12432.
15 M. Zhang and X. Wang, *Energy Environ. Sci.*, 2014, **7**, 1902.

16 K. Takanabe, K. Kamata, X. Wang, M. Antonietti, J. Kubota and K. Domen, *Phys. Chem. Chem. Phys.*, 2010, **12**, 13020.
17 C. Yang, W. Lee and H. Lin, Y. Dai, H. Chi and C. Chen, *RSC Adv.*, 2016, **6**, 40664.
18 Z. Zhang, D. Jiang, D. Li, M. He and M. Chen, *Appl. Catal. B. Environ.*, 2016, **183**, 113.
19 F. He, G. Chen, Y. Yu, S. Hao, Y. Zhou and Y. Zheng, *ACS Appl. Mat. Interfaces*, 2014, **6**, 7171.
20 X. Bai, C. Sun, S. Wu and Y. Zhu, *J. Mater. Chem. A*, 2015, **3**, 2741.
21 J. Zhang, G. Zhang, X. Chen, S. Lin, L. Möhlmann, G. Dołęga, G. Lipner, M. Antonietti, S. Blechert and X. Wang, *Angew. Chem.*, 2012, **124**, 3237.
22 J. Zhang, Y. Chen and X. Wang, *Energy Environ. Sci.*, 2015, **8**, 3092.
23 J. Qin, S. Wang, H. Ren, Y. Hou and X. Wang, *Appl. Catal. B. Environ.*, 2015, **179**, 1.
24 J. Zhang, M. Zhang, S. Lin, X. Fu and X. Wang, *J. Catal.* 2014, **310**, 24.
25 X. Fan, L. Zhang, R. Cheng, M. Wang, M. Li, Y. Zhou and J. Shi, *ACS Catal.*, 2015, **5**, 5008.
26 X. Fan, L. Zhang, M. Wang, W. Huang, Y. Zhou, M. Li, R. Cheng and J. Shi, *Appl. Catal. B. Environ.*, 2016, **182**, 68.
27 D. J. Martin, K. Qiu, S. A. Shevlin, A. D. Handoko, X. Chen, Z. Guo and J. Tang, *Angew. Chem., Int. Ed.*, 2014, **53**, 9240.
28 P. Wu, J. Wang, J. Zhao, L. Guo and F. E. Osterloh, *J. Mater. Chem. A*, 2014, **2**, 20338.
29 Y. Guo, F. Kong, C. Wang, S. Chu, J. Yang, Y. Wang and Z. Zou, *J. Mater. Chem. A*, 2013, **1**, 5142.
30 Y. Zhou, L. Zhang, J. Liu, X. Fan, B. Wang, M. Wang, W. Ren, J. Wang, M. Li and J. Shi, *J. Mater. Chem. A*, 2015, **3**, 3862.
31 J. Zhang, M. Zhang, C. Yang and X. Wang, *Adv. Mater.*, 2014, **26**, 4121.
32 J. Xu, F. Wu, H.-T. Wu, B. Xue, Y.-X. Li and Y. Cao, *Microporous Mesoporous Mater.*, 2014, **198**, 223.
33 Q. Gu, Z. Gao, H. Zhao, Z. Lou, Y. Liao and C. Xue, *RSC Adv.*, 2015, **5**, 49317.
34 S. Yang, Y. Gong, J. Zhang, L. Zhan, L. Ma, Z. Fang, R. Vajtai, X. Wang and P. M. Ajayan, *Adv. Mater.*, 2013, **25**, 2452.
35 F. Cheng, J. Yan, C. Zhou, B. Chen, P. Li, Z. Chen and X. Dong, *J. Colloid Interface Sci.*, 2016, **468**, 103.
36 S. N. Talapaneni, S. Anandan, G. P. Mane, C. Anand, D. S. Dhawale, S. Varghese, A. Mano, T. Mori and A. Vinu, *J. Mater.Chem.*, 2012, **22**, 9831.
37 B. Zhu, P. Xia, W. Ho and J. Yu, *Appl Surf Sci*, 2015, **344**, 188
38 W. Ho, Z. Zhang, W. Lin, S. Huang, X. Zhang, X. Wang and Y. Huang, *ACS Appl. Mater. Interfaces*, 2015, **7**, 5497.
39 Y. Chen, B. Wang, S. Lin, Y. Zhang and X. Wang, *J. Phys. Chem. C*, 2014, **118**, 29981.
40 Y. Zheng, L. Lin, X. Ye, F. Guo and X. Wang, *Angew. Chem., Int. Ed.*, 2014, **53**, 11926.
41 Y. Sui, J. Liu, Y. Zhang, X. Tian and W. Chen, *Nanoscale*, 2013, **5**, 9150.
42 J. Zhang, X. An, N. Lin, W. Wu, L. Wang, Z. Li, R. Wang, Y. Wang, J. Liu and M. Wu, *Carbon*, 2016, **100**, 450.
43 Q. Liang, Z. Li, X. Yu, Z.-H. Huang, F. Kang and Q.-H. Yang, *Adv. Mater.*, 2015, **27**, 4634.
44 Y. Kang, Y. Yang, L.-C. Yin, X. Kang, G. Liu and H.-M. Cheng, *Adv. Mater.*, 2015, **27**, 4572.

A table of contents entry

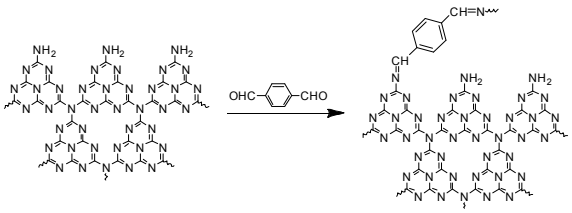

A novel and facile post-grafting strategy has been developed to construct aromatic heterocycle-grafted graphitic carbon nitridephotocatalysts.